UC Irvine
UC Irvine Previously Published Works

Title

An Assessment of HOx Chemistry in the Tropical pacific Boundary Layer: Comparison of Model Simulations with Observations Recorded During PEM Tropics A

Permalink

https://escholarship.org/uc/item/664043hg

Journal

Journal of Atmospheric Chemistry, 38(N3)

Authors

Blake, DR

Chen, G

Davis, D

et al.

Publication Date

2001

Copyright Information

This work is made available under the terms of a Creative Commons Attribution License, available at https://creativecommons.org/licenses/by/4.0/

Peer reviewed

eScholarship.org Powered by the California Digital Library
University of California

Journal of Atmospheric Chemistry **38:** 317–344, 2001.
© 2001 *Kluwer Academic Publishers. Printed in the Netherlands.*

An Assessment of HO_x Chemistry in the Tropical Pacific Boundary Layer: Comparison of Model Simulations with Observations Recorded during PEM Tropics A

G. CHEN[1], D. DAVIS[1], J. CRAWFORD[2], B. HEIKES[3], D. O'SULLIVAN[4], M. LEE[5], F. EISELE[6], L. MAULDIN[6], D. TANNER[1], J. COLLINS[2], J. BARRICK[2], B. ANDERSON[2], D. BLAKE[7], J. BRADSHAW[1], S. SANDHOLM[1], M. CARROLL[8], G. ALBERCOOK[8] and A. CLARKE[9]

[1]*Georgia Institute of Technology, Atlanta, GA, U.S.A.*
[2]*NASA Langley Research Center, Hampton, VA, U.S.A.*
[3]*University of Rhode Island, Narragansett, RI, U.S.A.*
[4]*U.S. Naval Academy, Annapolis, MD, U.S.A.*
[5]*Korea Ocean Research and Development Institute, Seoul, Korea*
[6]*National Center for Atmospheric Research, Boulder, CO, U.S.A.*
[7]*University of California at Irvine - Irvine, Irvine, CA, U.S.A.*
[8]*University of Michigan, Ann Arbor, MI, U.S.A.*
[9]*University of Hawaii, Honolulu, HI, U.S.A.*

(Received: 8 March 1999; accepted: 9 August 2000)

Abstract. Reported are the results from a comparison of OH, $H_2O_2CH_3OOH$, and O_3 observations with model predictions based on current HO_x–CH_4 reaction mechanisms. The field observations are those recorded during the NASA GTE field program, PEM-Tropics A. The major focus of this paper is on those data generated on the NASA P-3B aircraft during a mission flown in the marine boundary layer (MBL) near Christmas Island, a site located in the central equatorial Pacific (i.e., 2° N, 157° W). Taking advantage of the stability of the southeastern trade-winds, an air parcel was sampled in a Lagrangian mode over a significant fraction of a solar day. Analyses of these data revealed excellent agreement between model simulated and observed OH. In addition, the model simulations reproduced the major features in the observed diurnal profiles of H_2O_2 and CH_3OOH. In the case of O_3, the model captured the key observational feature which involved an early morning maximum. An examination of the MBL HO_x budget indicated that the $O(^1D) + H_2O$ reaction is the major source of HO_x while the major sinks involve both physical and chemical processes involving the peroxide species, H_2O_2 and CH_3OOH. Overall, the generally good agreement between model and observations suggests that our current understanding of HO_x–CH_4 chemistry in the tropical MBL is quite good; however, there remains a need to critically examine this chemistry when both CH_2O and HO_2 are added to the species measured.

Key words: hydroxyl radical, marine boundary layer, peroxides, photochemistry, tropical Pacific.

1. Introduction

Since the early 1970s, free radicals have been recognized as key components of tropospheric photochemistry (Levy *et al.*, 1971, 1972, 1974). Two of the most critical of these radicals are the hydroxyl, OH, and hydroperoxy, HO_2, species. As the most important tropospheric oxidant, OH reactions provide the main sink for most tropospheric trace gases, including the important greenhouse species, e.g., methane, methyl chloroform, and methyl bromide. The hydroperoxy radical, on the other hand, is believed to define one of the most important pathways for converting NO to NO_2. As such, it defines a major source of photochemically generated O_3. The photochemical processes that encompass the production, destruction, and interconversion of these radicals defines HO_x ($OH + HO_2$) chemistry, which is the principal focus of this paper.

A critical examination of HO_x chemistry has only recently become possible with the development of new experimental techniques for the direct measurement of OH and HO_2 (Eisele and Tanner, 1991, 1993; Mount, 1992; Tanner and Eisele, 1995; Harder *et al.*, 1997; Brune *et al.*, 1998). Heretofore, tests of fast photochemical mechanisms have been primarily confined to observational data for the photochemically controlled species NO_2, H_2O_2, and CH_3OOH (e.g., Trainer *et al.*, 1987; Chameides *et al.*, 1990; Liu *et al.*, 1992; Ridley *et al.*, 1992; Davis *et al.*, 1993; Fan *et al.*, 1994; Crawford *et al.*, 1996; Heikes *et al.*, 1992, 1996a,b; Penkett *et al.*, 1998, Ayers *et al.*, 1992, 1996). Historically, the results from these studies have been mixed, with those involving NO and NO_2 showing some of the largest disagreements between predictions and observations (e.g., Crawford *et al.*, 1996). However, more recent airborne studies, based on highly improved sampling of the NO_2 species, seemed to have resolved much of the earlier disagreement (i.e., Bradshaw *et al.*, 1999). Typically, better agreement has been found between predicted and observed H_2O_2 and CH_3OOH levels. It is not entirely clear, though, whether some significant element of this better agreement may simply reflect the fact that deposition loss rates for the peroxides have been adjusted over a substantial range to get agreement with the observations. Quite interestingly, in some cases the good agreement with respect to CH_3OOH has been accompanied by rather poor agreement between predictions and observations for CH_2O. This occurs, despite the strong coupling both species have to the photochemical oxidation of CH_4.

Overall, significant questions still persist concerning the H_xO_y family. Sources and sinks of HO_x have not been quantified. For example, for most environments coincident model and observational data are still lacking. Thus, questions remain about the importance of aerosol scavenging of HO_2 and nighttime chemical processes that might maintain significant levels of HO_2 in the troposphere. There also remain significant unresolved issues related to some of the more stable by-products of HO_x, radical chemistry. Included among these are BL deposition velocities, washout and rainout efficiencies, and aerosol scavenging of H_2O_2 and CH_3OOH.

Not surprisingly, HO_x related photochemistry tends to be most intense in a tropical marine BL setting, being strongly driven by both high UV solar irradiance and high levels of water vapor. Coincidently, it is the same setting that tends to generate the lowest diversity of free radicals, reflecting in no small measure the absence of high concentration levels of complex organic compounds. Thus, the remote marine BL defines an ideal environment in which to explore the details of HO_x chemistry. To date, one of the more extensive tests of this chemistry has been that reported by Thompson *et al.* (1993). This study was carried out using data recorded during the SAGA 3 ship cruise in the central equatorial Pacific. Comparisons were made between model calculated and observational values for both H_2O_2, and CH_3OOH. Since no direct observations were available for OH, these investigators resorted to indirect methods of comparison involving marine sulfur species such as dimethyl sulfide (DMS).

In the current investigation of HO_x chemistry, the remote marine boundary layer once again defines the test environment. The data analyzed here is that collected in the near vicinity of Christmas Island (2° N, 157° W) in the central tropical Pacific. This data was recorded during the P-3 B flight 7 of NASA's PEM-Tropics A field program.

2. Observations

The Christmas Island P-3 B local flight 7 represents the centerpiece of the data analyzed. This data set was unique in that: (a) it encompassed a Lagrangian sampling scenario which covered a significant fraction of a solar cycle; (b) it provided a comprehensive set of measurements of the critical species OH, O_3, H_2O_2, and CH_3OOH; and (c) it provided *in situ* measurements of the aerosol number/size distribution. During flight 7 both BL and buffer layer (BuL) altitudes were sampled. (Note: the term 'buffer layer' is used here to designate the atmospheric region between the top of the BL and the bottom of the lower free troposphere as recently defined by Russell *et al.* (1998).) There was also one vertical chemical sounding recorded up to an altitude of 4.5 km in the lower free troposphere. The BL sampling sequence started approximately 360 km southeast of Christmas Island with the aircraft flying a series of circular sampling patterns while drifting with the wind. The mean motion of the aircraft was along a heading of $\sim$130°. The time history of flight 7 study covered the period of 5:30 to 13:30 hrs, local sun time. For a more detailed description of the sampling methodology, the reader is referred to Davis *et al.* (1999).

In addition to the HO_x species listed above, also recorded were measurements of the critical species/parameters CO, O_3, NMHC's (non-methane hydrocarbon), temperature, UV irradiance, and dew point. Due to technical problems with the chemiluminescent NO analyzer at the time of flight 7, the only available BL NO values for this analysis were those reported by Bradshaw *et al.* (1999). The latter measurements were made 10 days following the P-3B flight 7 using a TP-LIF

(Two Photon Laser Induced Fluorescence) NO sensor mounted on a second PEM-Tropics A aircraft, the NASA's DC-8. This DC-8 Christmas Island BL fly-by resulted in an average NO value of 3 pptv. The latter average for NO is consistent with those previously reported by Torres and Thompson (1993) for the same general region as recorded during the SAGA 3 ship cruise.

The airborne measurement of OH was carried out using the select-isotope chemicalionization mass spectrometry (SI/CI/MS) technique. The data collection rate was set at 30 sec; however, for some analysis these data were also blocked as 10 min time intervals to improve the S/N (signal/noise) ratio. At the latter resolution, the limit of detection (LOD) was 2×10^5 molec/cm^3. Details concerning the SI/CI/MS technique have been previously reported by Eisele and Tanner (1991, 1993). The species H_2O_2 and CH_3OOH were measured using a grab sampling technique in conjunction with HPLC (high pressure liquid chromatography) analysis as previously described by Lee *et al.* 1995). The typical time resolution for the peroxides measurements was $\sim$5 min. The LOD for H_2O_2 and CH_3OOH was 15 and 25 pptv, respectively. For flight 7, the reported uncertainty in the individual measurements of H_2O_2 averaged to $\pm$12%, while for CH_3OOH it was $\pm$13%. The 'dry' aerosol number/size distribution measurement was carried out using both a radial differential mobility analyzer (RDMA) and an optical particle counter (OPC). The size range covered by the RDMA was $0.01 - 0.148$ μm and that for the OPC covered 0.148 to 6 μm. The typical time resolution for the RDMA was 40 sec while that for the OPC ranged from 120 sec to 540 sec. Details concerning the aerosol measurements have been previously reported by Clarke *et al.* (1999). For all other measurements not discussed here, details concerning time resolution, detection methodology, and LOD levels can be found in the PEM-Tropics A 'Operational Overview' paper by Hoell *et al.* (1999).

Boundary layer levels of OH, UVZ (the zenith looking UV), O_3, H_2O_2, and CH_3OOH as a function of local sun time are shown in Figures 1(a, b). All data shown in these figures is for BL altitudes only. Lines drawn through the data are polynomial trend lines. As shown in Figure 1(a), OH is seen rapidly increasing with increasing UV irradiance, peaking at $\sim8\times10^6$ molec/cm^3 near solar noon, and then slowly decreasing toward the end of the mission at 13:30 hrs. Figure 1(b) shows a similar trend in the levels of H_2O_2 and CH_3OOH; however, in both cases the minimums are not observed until nearly an hour following sunrise. These minimums are followed by modest increases throughout the late morning into early afternoon, as would be expected for a longer lived photochemical species. The magnitude of the increase over the early morning minimum is estimated at $\sim$400 pptv for H_2O_2 and 330 pptv for CH_3OOH. Although these diurnal trends are somewhat similar to those reported by Thompson *et al.* (1993) for SAGA 3 observations, the PEM-Tropics A observations have much higher diurnal averaged values (i.e., a factor of $\sim$2 for H_2O_2 and $\sim$1.5 for CH_3OOH) as well as greater amplitudes (i.e., a factor of $\sim$2 for both H_2O_2 and CH_3OOH). For O_3, although considerable fluctuation is seen in the data, a clear trend is still evident which shows O_3 maximizing near 10:00 hrs

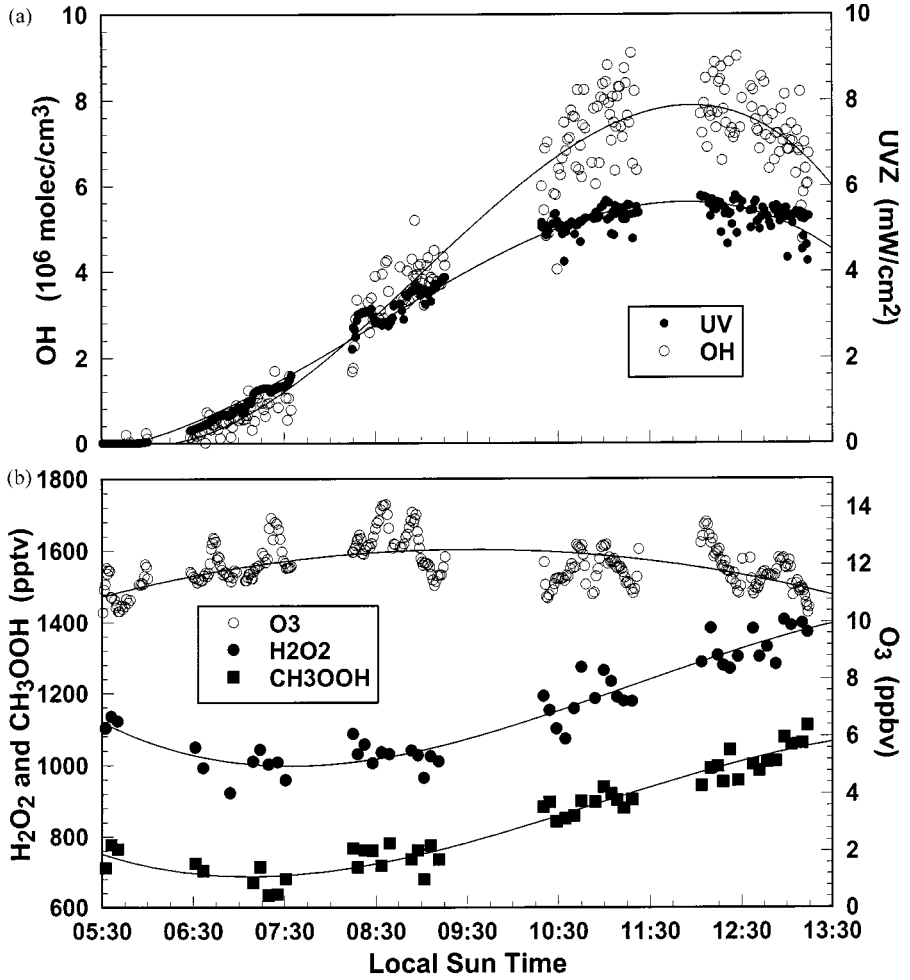


Figure 1. Time series plots for (a) OH and UVZ and (b) O_3, H_2O_2 and CH_3OOH. Trend lines shown represent polynomial fit. Data recorded in the vicinity of Christmas Island on August 24th, 1996.

local sun time, followed by steady decreases up to the time that sampling ended. Similar O_3 trends have previously been reported in the central tropical Pacific by Thompson *et al.* (1993) and Clarke *et al.* (1996). A quick inspection of the relative trends for O_3, H_2O_2, and CH_3OOH suggests that O_3 is generally anticorrelated with the peroxides. The anticorrelation between these species has been previously reported for remote marine BL conditions by Ayers *et al.* (1992).

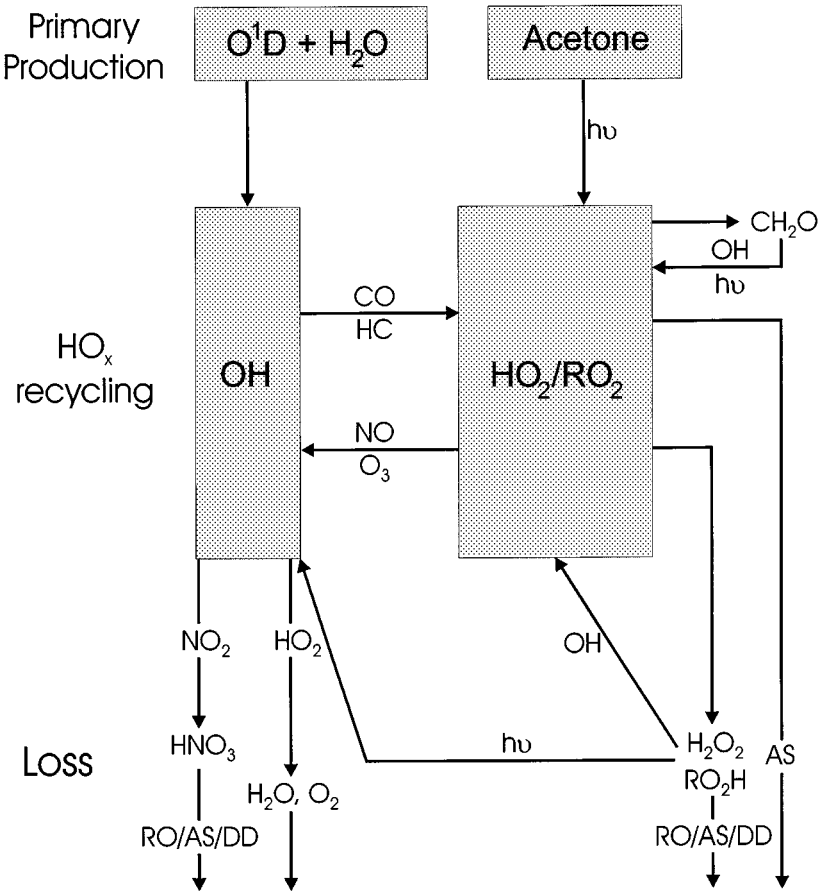


Figure 2. Schematic diagram of HO_x sources, sinks, and recycling for remote marine BL conditions. RO = rain out, AS = aerosol scavenging, and DD = dry deposition

3. HO_x Chemistry and Model Description

For illustration purposes we have summarized in Figure 2 some of the more important chemical characteristics of BL and BuL HO_x chemistry. The three major components of the HO_x chemical cycle shown are: primary production, HO_x recycling, and HO_x sinks. Primary production in the form of reaction (R1) is clearly the dominant photochemical source of HO_x at low altitudes in the tropics:

$$O(^1D) + H_2O \rightarrow 2\,OH \qquad \text{(R1)}$$

Only very minor contributions are made at these altitudes from acetone photolysis, (R2),

$$CH_3COCH_3 + h\nu \rightarrow CH_3CO + CH_3 \qquad \text{(R2)}$$

The recycling and secondary production of OH is seen as primarily driven by reactions (R3) → (R10).

$$OH + CO \rightarrow H + CO_2\,, \tag{R3}$$

$$H + O_2 + M \rightarrow HO_2\,, \tag{R4}$$

$$OH + CH_4 \rightarrow H_2O + CH_3\,, \tag{R5}$$

$$HO_2 + NO \rightarrow OH + NO_2\,, \tag{R6}$$

$$HO_2 + O_3 \rightarrow OH + 2\,O_2\,, \tag{R7}$$

$$HO_2 + HO_2 \rightarrow H_2O_2 + O_2\,, \tag{R8}$$

$$H_2O_2 + h\nu \rightarrow 2\,OH\,, \tag{R9}$$

$$H_2O_2 + OH \rightarrow HO_2 + H_2O\,. \tag{R10}$$

Both CH_3 radicals and the subsequent carbon oxidation product CH_3OOH contribute to the secondary production and recycling of OH, but as discussed in section 4.2 their contribution for tropical BL conditions is significantly less than that defined by reactions (R6), (R7), and (R9).

The NMHC species C_2H_4, C_2H_6, C_3H_8, etc. contribute still less. A summary of all reactions included in our analyses (i.e., 250) can be found in earlier related work by our group, see, for example, Crawford *et al.* (1999a).

As illustrated in the reaction sequence (R3) → (R10), one of the major sources of HO_2 is the reaction of OH with CO (R3). In addition, reactions between the organic peroxy radicals CH_3O_2 and RO_2 with NO also contribute. The typical by-product from the latter reactions is the formation of the aldehyde species HCHO and RCHO. As shown in Figure 2, via direct photolysis and/or reaction with OH both aldehyde species can lead to the subsequent forination of HO_2 radicals. Under typical tropical marine boundary layer conditions (i.e., NO $\leqslant$ 3 pptv), one HCHO molecule can, on average, generate $\sim$0.4 HO_2 radicals. However, considering the entire oxidation sequence for CH_4 and its intermediate products (e.g., CH_3OOH, HCHO), there would result a total loss of HO_x radicals, e.g., $\sim$1.5 HO_x radicals per CH_4 molecule oxidized.

The removal of HO_x radicals from the tropical marine BL is quite interesting in that as illustrated in Figure 2 it occurs primarily through the formation and loss of peroxide species and HNO_3. The one exception to the above statement involves reaction (R11) which defines a radical-radical termination step for OH and HO_2. The peroxide species as well as HNO_3 are removed from the BL by physical processes which include: rainout, dry and wet aerosol scavenging, and dry deposition to the

ocean surface (RO/AS/DD). These sink related processes are summarized below in the form of reactions (R12) → (R16):

$$OH + HO_2 \rightarrow H_2O + O_2\,, \tag{R11}$$

$$H_2O_2(RO/AS/DD) \rightarrow \text{Removal}\,, \tag{R12}$$

$$OH + NO_2 + M \rightarrow HNO_3\,, \tag{R13}$$

$$HNO_3(RO/AS/DD) \rightarrow \text{Removal}\,, \tag{R14}$$

$$HO_2 + CH_3O_2 \rightarrow CH_3OOH + O_2\,, \tag{R15}$$

$$CH_3OOH(RO/AS/DD) \rightarrow \text{Removal}\,. \tag{R16}$$

More speculative has been the proposal by some investigators (e.g., Mauldin *et al.*, 1998; Cantrell *et al.*, 1996) that the relatively high sticking coefficient for HO_2 radicals might lead to a significant loss on aqueous aerosols. If true, this also could define another loss pathway for tropospheric HO_x radicals, e.g., (R17)

$$HO_2 + \text{Aqueous Aerosol} \rightarrow \text{Removal} \tag{R17}$$

An interesting aspect of the HO_2 radical removal process (R17) is that it is in direct competition with the major HO_2 self reaction (R8). The latter reaction, leading to the formation of H_2O_2, is seen as quadratically dependent on HO_2 levels. Thus, the availability of H_2O_2 measurements in conjunction with aerosol number/size distributions potentially provides a means for testing the importance of process (R17), e.g., see discussion in section 4.3.

Two basic types of models were used in the current study: a time dependent (TD) photochemical box model, and a photostationary state (PSS) point model. The TD model was used to simulate the large scale diurnal variations in O_3, H_2O_2, CH_3OOH, CH_2O, and OH, while the PSS model provided values for the short lived species OH and HO_2 for specific times and specific sampling locations along a given flight track. These models have been described in detail in previous publications (Davis *et al.*, 1993, 1996; Crawford *et al.*, 1996, 1997a, b, 1999a). As also noted earlier in the text, a complete listing of all reactions used in the current model has been provided in Crawford *et al.* (1999a). We note that for longer lived species such as the peroxides, all simulations were based on the assumption that the species reached quasi-steady state. In the case of the peroxides, since their lifetimes were less than one day, the error resulting from this assumption should have been reasonably small.

Other modifications made to the TD model for this study involved the inclusion of a parameterized vertical transport term to quantify the mass exchange between the BuL and BL. This was of particular importance in addressing budget

issues for the reasonably long lived photochemical species such as O_3, H_2O_2, and CH_3OOH. This term has an identical form to that adopted in a related study involving DMS oxidation (i.e., also based on flight 7) as described in detail by Davis *et al.* (1999). With this modification the generic form of our mass balance equation can be expressed as in Equation (1):

$$\frac{\mathrm{d}[X]}{\mathrm{d}t} = F(X) - D(X) + \frac{M}{h}\left([X]_{\mathrm{BuL}} - [X]\right) . \tag{1}$$

Here, X represents a generic photochemical species (e.g., O_3, H_2O_2, and CH_3OOH). $F(X)$ is the photochemical formation term for species X; while $D(X)$ is the total loss frequency term which includes both photochemical destruction of species X as well as its physical removal. The last term on the right hand side of Equation (1) is the parameterized vertical transport term for the mass exchange of species X between the BuL and BL. Here, 'M' represents the mixing parameter previously defined by Davis *et al.* (1999), 'h' is the boundary layer height, and $[X]_{\mathrm{BuL}}$ is the BuL mixing ratio for species X. From the mathematical form of this term, the sign of the net mass flux of X is seen as driven by its mixing ratio difference between the two layers. This reflects the fact that in the case of flight 7 the BuL is intermittently turbulent and the mass exchange between the BL and BuL is bi-directional. The rate of the bi-directional exchange is defined by the mixing parameter 'M' which has dimension of velocity. In this study, the magnitude of 'M' (i.e., 1.2 cm/sec) was taken from an analysis of the DMS vertical distribution as reported by Davis *et al.* (1999). The high value for M reflects the presence of wide-scale shallow convection in the sampling region both before and during flight 7.

Photolysis rate coefficients were evaluated from a DISORT 4-stream implementation of the NCAR TUV (Tropospheric Ultraviolet-Visible) radiative transfer code (S. Madronich, private communication). A more detailed description of the photolysis rate coefficient calculations can be found in Crawford *et al.* (1999b). Of the 12 non-hydrocarbon photochemical rate coefficients used in this analysis for all but one of these the quantum yield and absorption cross section data were those reported in DeMore *et al.* (1997). The one exception was the quantum yield data for $O(^{\prime}D)$ formation. In this particular case the newer quantum yield data of Talukdar *et al.* (1998) were used. All photolysis rate coefficients were adjusted to reflect the solar/cloud conditions encountered during sampling. This adjustment was based on both downward and upward looking UV Eppley measurements and has previously been given the name in our model 'cloud correction factor', CCF. CCF has been previously defined by Davis *et al.* (1993, 1996), Chen, (1995), and Crawford *et al.* (1996, 1997, 1999b). In this study, its value was determined from the ratio of $j(NO_2)$ derived from Eppley UV measurements to that calculated for clear sky conditions by the NCAR TUV. Although there are some distinct spectral differences between $j(NO_2)$ and $j(O(^{\prime}D))$, Crawford *et al.* (1999b) have shown that there is no significant differences in the CCF values estimated from $j(NO_2)$

Table I. Summary of photochemical input parameters

Variable	Median value
LAT (°N)	1.4
LON (°E)	–155.0
ALT (km)	0.17
Temperature (°C)	24.6
Pressure (mb)	992
Dew point (°C)	21.6
O_3 (ppbv)	11.9
CO (ppbv)	58.2
NO (pptv)	3
C_2H_6 (pptv)	293
C_3H_8 (pptv)	12
H_2O_2 (pptv)	1164
CH_3OOH (pptv)	864
O_3 Column Density (DU) [a]	252

[a] Data retrieved from http://jwocky.gsfc.nasa.gov/ (McPeters *et al.*, 1998).

versus $j(O(^1D))$. For the PSS runs, individual CCF values were assigned to each point model calculation, while for the TD runs an averaged CCF value over the entire flight was adopted to constrain the model output. The same CCF value was applied to all j-values.

4. Model Results and Discussion

4.1. OH OBSERVATIONS AND SIMULATIONS

As noted earlier in the text, both TD and PSS models were used to assess the level of agreement between theoretical predictions and observations. These results are shown in Figures 3 and 4(a, b). In Figure 3, TD model profile is compared against the flight 7 OH observations. (The model profile was constrained by median values of all input parameters, including the peroxide species H_2O_2 and CH_3OOH, as listed in Table I). The solid circles and associated error bars represent average values and the associated standard deviation obtained from averaging the observational data over 10 min blocks. The solid and dashed lines in Figure 3 represent the output from our 'standard model' together with our estimate of the most probable systematic error in the modeled OH profile. As seen from Figure 3, the simulated and observed profiles lie well within the cited uncertainties.

The systematic error cited for our model profile reflects the potential error that could result from the accumulated uncertainties in all j and k values used in the model. This composite error was evaluated using Monte Carlo calculations sim-

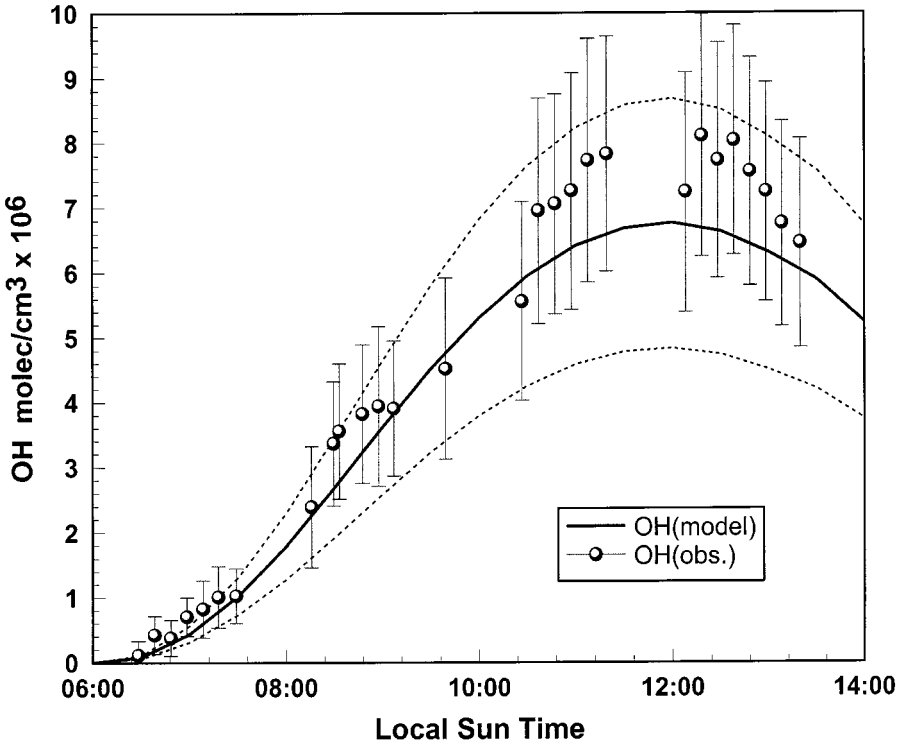


Figure 3. Comparison of TD model simulated and observed OH profiles. Symbols give the mean and overall uncertainty including standard deviation for OH data averaged over 10 min intervals (The quoted 10 min. precision is about 10%.) and 20% potential systematic error. Solid line indicates the model calculated profile with dashed lines encompassing the overall uncertainties including ±12% of random error and ±25% potential systematic error due to rate constant uncertainties.

ilar to those described by Thompson and Stewart (1991), Davis *et al.* (1993) and Crawford *et al.* (1997b). As in earlier applications describing this approach, we have taken the uncertainties in the individual gas kinetic and photochemical rate coefficients for BL tropical conditions to be those cited by DeMore *et al.* (1997). As shown in Figure 3 the final model estimated systematic error based on this approach is computed to be 25%. Other possible systematic errors that must be considered in the comparison include those related to the OH observational data themselves as well as those associated with the observational values used for NO. The first of these uncertainties is tied to the absolute calibration of the OH measurement system. This error has been cited as being as high as 20% (1σ) of the reported value (Mauldin *et al.*, 1999). Regarding NO, since a value was assumed for flight 7 based on after-the-fact measurements, sensitivity tests were carried out using a wide range of possible NO values (e.g., 1, 6, and 9 pptv). The results showed that relative to our standard model, which used 3 pptv, the OH level decreased by 3% at 1 pptv and increased by 5 and 11% for NO values of 6 and 9 pptv. Thus, the

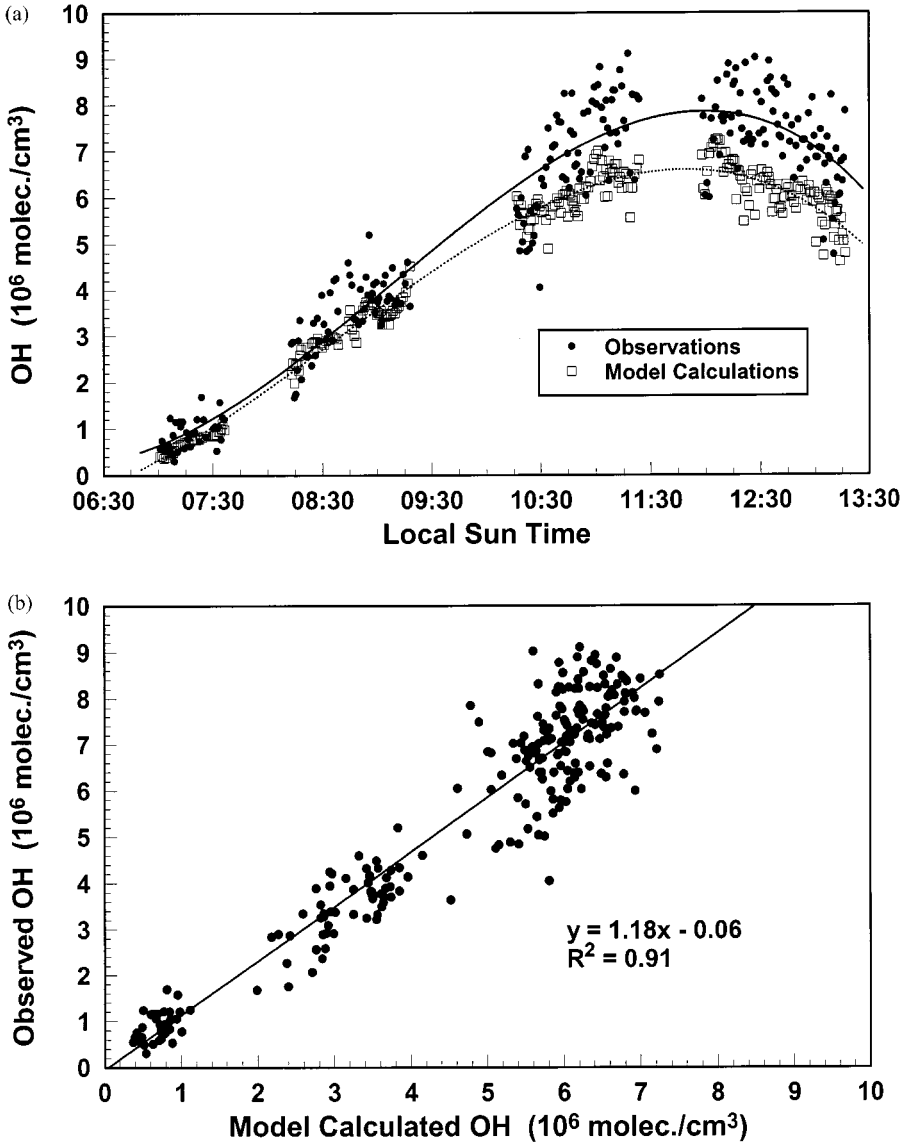


Figure 4. (a) Comparison of PSS model simulated and observed OH profiles. Solid line and dashed line denote polynomial trend lines for the observation and model simulation, respectively. (b) Correlation plot of PSS model results vs OH observations.

potential systematic error from this source may be viewed as quite modest relative to the uncertainty estimated for the absolute calibration of the OH sensor.

The above cited potential systematic errors may be contrasted to our current estimate of the random error associated with our model calculations, e.g., $\pm 12\%$. This error estimate was based on the uncertainties associated with the individual observational input parameters, i.e., CO, H_2O, O_3 and the CCF using propagation

of error techniques. As seen from Figure 3 the combined instrument precision and natural OH fluctuations resulted in an overall random error ranging from over 40% in the morning to ∼12% near noon. Most of this error was due to the natural variability in OH. These results suggest that future comparisons of models with observational data should focus on reducing the magnitude of the systematic errors in the observations and model calculations.

Comparisons of the PSS model results with the OH observations are shown in Figures 4(a, b). In Figure 4(a) each solid circle represents the average observed OH value integrated over a 1 minute time interval. Similarly, the PSS model results are based on 1 minute observational data (i.e., O_3, CO, H_2O, H_2O_2, CH_3OOH and CCF). The 1σ uncertainty the OH observational data is about $\pm$ 15%. Recall, a similar magnitude of random error (i.e., $\pm$ 16%) was estimated for the model results.

Not surprisingly, the PSS results show quite good agreement with the TD OH profile. Recall, that the PSS calculations were modulated by *in situ* CCF values while the TD model simulations were based on an overall CCF value, averaged from data for the whole region. The PSS results like those from TD model suggest that current model mechanisms used to descibe tropical MBL HO_x chemistry give a quite good representation of this chemistry, i.e., within 15 to 20%. This point is further illustrated here in the form of Figure 4(b) which shows the individual PSS model and observational data plotted against each other. A regression analysis of these data gives an 'R^2' value of 0.91 and a slope of 1.18.

4.2. OH BUDGET AND HO_x SOURCES AND SINKS

Of considerable importance in any quantitative examination of HO_x chemistry is an assessment of the relative importance of all major formation and loss pathways for OH. Collectively, these processes define the level of OH at any given time and location and ultimately play a major role in also defining the major sources and sinks for the HO_x family taken as a whole. Using the earlier TD modeling results, we show in Tables II(a, b) our estimation of the 24 hour averaged values for the source and sink terms making up the OH budget. Also shown in summarized form are the averages for the major sources and sinks for HO_x. As related to OH, it can be seen that formation is dominated by the reaction of $O(^1D)$ with H_2O (R1), comprising 81% of the total. The remainder, defined here as recycled HO, is made up of the photolysis of H_2O_2, CH_3OOH (R9, R10), and reaction of HO_2 with O_3 and NO, (R7) and (R6). Their respective contributions are indicated as 8%, 2%, 5%, and 4%, respectively. In contrast to formation, OH loss pathways are spread over several reactions. The two most important of these are (R3) and (R5) involving the reaction of OH with CO and CH_4. Collectively, these two processes define 61% of the total OH loss. Reaction with CH_3OOH, H_2, CH_2O, H_2O_2, HOD and O_3 contribute 11%, 9%, 7%, 6%, 4%, and 2%, respectively, and define the remainder of the OH loss.

Table IIa. Summary of OH formation and destruction

Formation	Percent contribution	Destruction	Percent contribution
$O(^1D) + H_2O$	81%	OH + CO	34%
$H_2O_2 + h\nu$	8%	$OH + CH_4$	27%
$HO_2 + O_3$	5%	$OH + CH_3OOH$	11%
$HO_2 + NO$	4%	$OH + H_2$	9%
$CH_3OOH + h\nu$	2%	$OH + CH_2O$	7%
		$OH + H_2O_2$	6%
		$OH + HO_2$	4%
		$OH + O_3$	2%
Total	100%		100%

Table IIb. Summary of HO_x sources and sinks

Sources	Flux[a] divergence	Percent contribution	Sinks	Flux[a] divergence	Percent contribution
Photochemical sources			$OH + HO_2$	1.6	8%
$O(^1D) + H_2O$	16.0	80%	H_2O_2 chemistry	7.6	39%
Transport sources			CH_4 chemistry	10.6	53%
$F_{H_2O_2}$	1.9	10%			
F_{CH_3OOH}	1.9	10%			
Total	19.8	100%		19.8	100%

Note: HO_x losses through H_2O_2 chemistry is equivalent to $2(k_{SL}[H_2O_2] + k[OH][H_2O_2])$. $k_{SL}(H_2O_2) = 9.8 \times 10^{-6}$ s^{-1} (estimated in this work); $k(OH + H_2O_2) = 1.7 \times 10^{-12}$ cm^3 molec.$^{-1}$ s^{-1} (DeMore *et al.*, 1997).

HO_x losses through CH_4 chemistry is equivalent to $2(k_{SL} + k[OH])[CH_3OOH]$. $k_{SL}(CH_3OOH) = 1.1 \times 10^{-5}$ s^{-1} (estimated in this work); $k(OH + CH_3OOH) = 7.4 \times 10^{-12}$ cm^3 molec.$^{-1}$ s^{-1} (DeMore *et al.*, 1997).

[a] Both source and sink strength are diel averages and given in 10^5 molec. cm^{-3} s^{-1}.

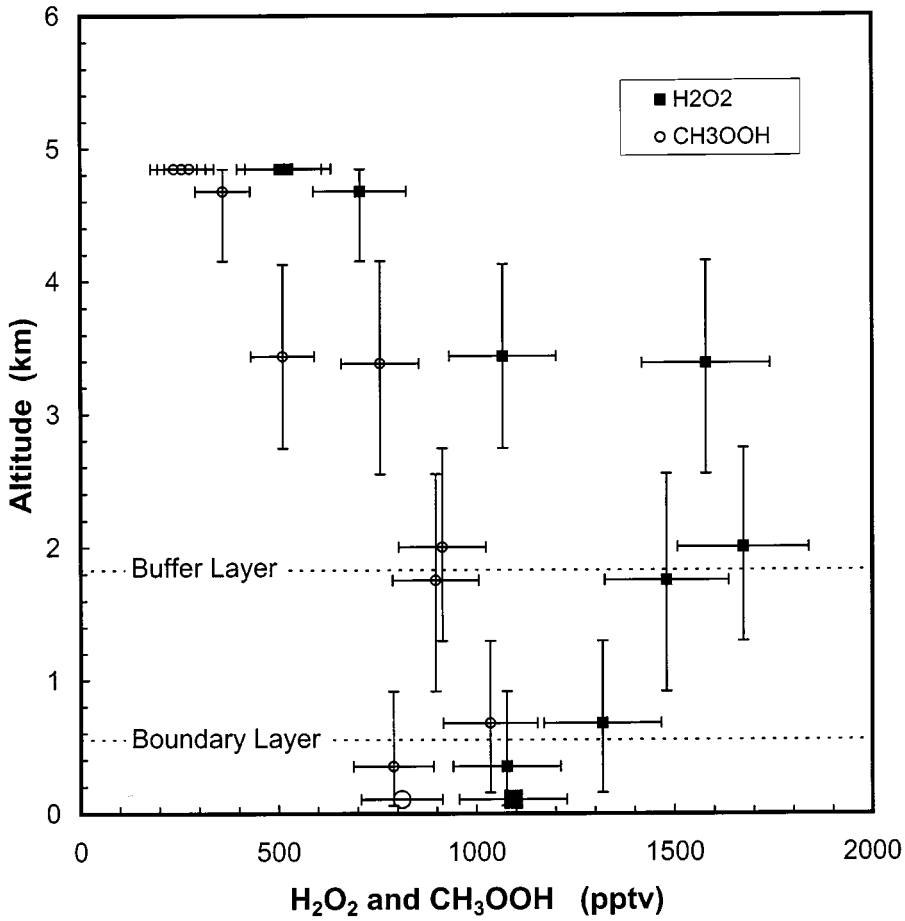


Figure 5. Vertical profiles for observed H_2O_2 and CH_3OOH. Horizontal bars represent reported measurement uncertainties and vertical bars denote the range of aircraft altitude covered by each measurement. The larger symbols at the bottom of the figure are averages for multiple measurements taken from horizontal flight legs.

Considering HO_x sources and sinks, the TD results shown in Table II(b) again point to reaction (R1) as the single dominant source for the tropical MBL. Acetone photolysis (not shown) conprises less than 1% of the total. Table II(b) indicates that other than reaction R1, transport of H_2O_2 and CH_3OOH from the BuL to the BL accounts for most of the remaining source, estimated here at 20%. As discussed in Section 3, vertical transport terms were introduced into our TD model to account for the exchange of mass between the BL and BuL. BuL peroxide levels were found to be significantly higher than those in the BL, e.g., see Figure 5.

HO_x losses in the MBL primarily appear in the form of surface deposition and scavenging processes. The one exception is R11, involving the reaction of HO_2 with OH to form the stable terminal species H_2O and O_2. However, this process

accounts for only 8% of the total. As noted in Section 3, the most important HO_x losses typically occur as a result of the physical removal of H_2O_2, HNO_3, and CH_3OOH. Of the species listed, for remote marine BL conditions the levels of NO_x are typically so low as to relegate HO_x losses to negligible levels. For the peroxide species H_2O_2 and CH_3OOH, HO_x losses can be reduced down to two general loss terms:

$$2\left(k_{\mathrm{RO/AS/DD}}\,[\mathrm{H_2O_2}] + k_{\mathrm{R1O}}\,[\mathrm{OH}]\,[\mathrm{H_2O_2}]\right) \tag{L1}$$

$$2\left(k_{\mathrm{RO/AS/DD}}\,[\mathrm{CH_3OOH}] + k_{\mathrm{CH_3OOH}}\,[\mathrm{OH}]\,[\mathrm{CH_3OOH}]\right)\ . \tag{L2}$$

(Note, L2 is an approximation to the net effect of CH_4 chemistry under remote tropical BL conditions. Thus, the coefficient of 2 can best be understood in terms of two HO_x radicals being required to form each CH_3OOH that is lost.)

The term Ll, related to losses through the H_2O_2 species, is seen in Table II(b) as accounting for 39% of the BL HO_x loss; whereas, L2 involving the peroxide species CH_3OOH contributes 53% of the total. For Ll the physical removal term involving $k_{\mathrm{RO/AS/DD}}$ is the dominant term, accounting for 75% of the total. By contrast, for L2 both the physical and chemical removal terms make significant contributions, e.g., 43% and 57%, respectively. These results suggest that to accurately assess the tropical BL HO_x budget it is crucial to have both reliable measurements of the peroxide species as well as reliable OH rate coefficients. Noteworthy here is the current large uncertainty in the OH/CH_3OOH rate coefficient of a factor of 1.5 (DeMore *et al.*, 1997).

Although the HO_x source/sink budget shown in Table II(b) reflects the results from our 'standard' model, it does not address the issue raised earlier related to the possible importance of HO_x radical losses to aerosols, e.g., R17. Based on lifetime considerations, of the two HO_x radicals that might be considered here (i.e., OH and HO_2), HO_2 is clearly the most likely one to be affected by aerosols. Assessing this loss, however, requires a reliable value for the sticking coefficient, α, especially for aqueous aerosols. In fact, the sticking coefficient α_{HO_2} has been previously measured in the laboratory by Mozurkewich *et al.* (1988) and Hanson *et al.* (1992). Mozurkewich *et al.* reported a value of 0.2 for wet particles containing NH_4HSO_4; while Hanson *et al.* provided lower limit values for pure H_2O and for H_2SO_4 surfaces of 0.01 and 0.05 to 0.1, respectively. In this study, we assumed a wide range of values (i.e., 0.0, 0.2, 0.4, and 1.0) since clearly its value appears to be a strong function of the chemical aerosol type. It should also be recognized that aerosol scavenging of HO_2 radicals may very well be a reversible process (Chameides and Davis, 1982; Heikes and Thompson, 1983). If this were true, the HO_2 sticking coefficient may not be the controlling factor of its net removal. In the discussion that follows, we have made the simplifying assumption that the process is irreversible.

For the flight 7 data, use of the Fuchs and Sutugin Equation (Fuchs and Sutugin, 1970), in conjunction with the observed aerosol number/size distribution, provided

for an initial assessment of the first order HO_2 loss to aerosols. The values estimated here were 0.0, 1.3, 2.3, and 4.2×10^{-3} sec^{-1}, respectively. When combined with our model estimated level of HO_2, we found that the highest aerosol scavenging loss rate was nearly a factor 4 times higher than the value cited in Table II(b) for reaction R11. Expressed in terms of the budgets for HO_x and HO_2, this loss rate was equivalent to ~30% of the current estimate of the total HO_x sink and ~40% of that for HO_2. Furthermore, model generated HO_2 levels were found to be substantially reduced, e.g., 27%. Because of the quadratic dependence of H_2O_2 on HO_2, this reduction is also found to have a significant impact on the levels of H_2O_2. (Note, a more in-depth discussion of these results is provided in the text below.)

4.3. H_2O, AND CH_3OOH ANALYSIS

As noted earlier, a comparison of model simulated profiles for H_2O_2 and CH_3OOH with observational data provides one method of assessing our current level of understanding of HO_x chemistry, particularly as related to the radical species HO_2 and CH_3O_2. In this study, the model assessment involving H_2O_2 and CH_3OOH was carried out using mass conservation Equation (2):

$$\frac{\mathrm{d[POX]}}{\mathrm{d}t} = \mathrm{P(POX)} - \mathrm{L(POX)[POX]} - k_{\mathrm{SL}}\mathrm{[POX]} + \frac{M}{h}\left(\mathrm{[POX]_{BuL}} - \mathrm{[POX]}\right). \quad (2)$$

Here, 'POX' represents either H_2O_2 or CH_3OOH; P(POX) and L(POX) are the photochemical formation rate and loss frequency terms for the species 'POX'; and the quantity 'k_{SL}' defines the first order loss of the 'POX' species due to rainout, aerosol scavenging, and dry deposition to the ocean surface. As discussed in Section 3, the final term in Equation (2) treats in parameterized form the vertical transport of mass between the BuL and BL.

In Figure 5, the data for both H_2O_2 and CH_3OOH are shown plotted as function of altitude. Also given in this figure are the BL top of 0.55 km (defined by the vertical break point in the potential temperature vertical profile) and the BuL top of 1.8 km (defined as the inversion point in the vertical temperature profile) (see Davis *et al.*, 1999). As shown in the Figure, H_2O_2 levels are about 315 pptv higher in the BuL. Similarly, on average, BuL CH_3OOH is ~165 pptv higher. Following a similar approach as used earlier in the OH analysis, model simulations were used to generate diurnal profiles of H_2O_2 and CH_3OOH. (Note, median values of all input parameters used in these runs are those shown in Table I). In these runs the model was constrained with real time OH observations; and, as discussed in Section 3, the value of '*M*' (1.2 cm/sec) was that derived by Davis *et al.* (1999).

Concerning the BuL analysis, although the sampling was more limited for this vertical zone (5 sampling runs over a time span of 6 hours), diurnal profiles for the peroxides were still based on independent modeling simulations constrained by these BuL observations. The assumption was further made that no significant transport occurred between the BuL and the lower free troposphere, an assumption

that was reflected in an observed sharp drop in concentration levels of all surface released marine species such as DMS.

Figures 6(a, b) show the results from the BL H_2O_2 and CH_3OOH model simulations together with the corresponding observational data. The two curves shown in each figure reflect our use of different values for the first order physical loss rate for each peroxide, e.g., k_{SL}. The lower curve is based on a k_{SL} value that is nearly an order of magnitude higher than that derived from the observational data (e.g., see discussion later in text). This value assumes that the sticking coefficients, $\alpha_{H_2O_2}$ and α_{CH_3OOH}, control the aerosol scavenging rate. Sticking coefficients at 298 K for aqueous droplets have been reported for the peroxides by Worsnop *et al.* (1989) and Magi *et al.* (1996), e.g., 0.07 for H_2O_2 and $\geqslant$0.04 for CH_3OOH. Given these values and the number/size distribution for aerosols during flight 7 (median total surface area = 75 $\mu m^2/cm^3$ (Davis *et al.*, 1999)), the first order non-reversible scavenging rate coefficients were determined to be 5.8×10^{-4} sec^{-1} for H_2O_2 and $\geqslant 3.5 \times 10^{-4}$ sec^{-1} for CH_3OOH. The fact that the fit to the data in Figures 6(a, b) is so poor when using these high k_{SL} values suggests that the assumption that the loss of peroxides to sea-salt aerosol is controlled by the value of $\alpha_{H_2O_2}$ and α_{CH_3OOH} is most likely in error. For example, Ayers *et al.* (1996) have suggested that the uptake of H_2O_2 may be limited by its aqueous phase reaction with SO_2. If true, since SO_2 levels are typically more than 10 times lower than BL H_2O_2 levels for remote marine conditions, aerosol scavenging, as controlled by $\alpha_{H_2O_2}$ and α_{CH_3OOH}, would give unrealistic estimates for the loss of peroxide species. This is consistent with the results from earlier modeling and laboratory studies which have indicated that the magnitude of the sticking coefficient was not the limiting factor for aerosol scavenging of H_2O_2 (Schwartz, 1981, 1984, 1986, 1988; Chameides, 1984; Jacob, 1986; Worsnop *et al.*, 1989).

With regards to the upper model profile shown in Figures 6(a, b), as noted above first order removal rates for H_2O_2 and CH_3OOH were derived from the peroxide data itself. For this scenario, k_{SL} was left as an adjustable parameter in Equation (2). Thus, the final values were dictated by the best fit between the model simulated profiles and those defined by the observations. The goodness of the fit was determined from the minimum in the chi-squared values. As shown in the Figures 6(a, b), the k_{SL} values derived from this type of analysis appear to reproduce the observations quite well. The final values were 9.8×10^{-6} sec^{-1} for H_2O_2 and 1.1×10^{-5} sec^{-1} for CH_3OOH. These values are seen as being within 30% of those previously reported by Ayers *et al.* (1992); Thompson *et al.* 1993); Heikes *et al.* (1996b). We estimate that the uncertainty in our assessment of k_{SL} is a factor of 1.5.

As discussed earlier in the text, the value of k_{SL} derived here represents the total first order loss of peroxides from all processes, e.g., washout (WO), rainout (RO), dry deposition as well as scavenging by all forms of aerosols. This raises the question whether the individual contributions making up the total can be evaluated independently. In the case of flight 7 we have been able to take advantage of the fact that there were limited, but significant, BuL peroxide observations. Thus, in this

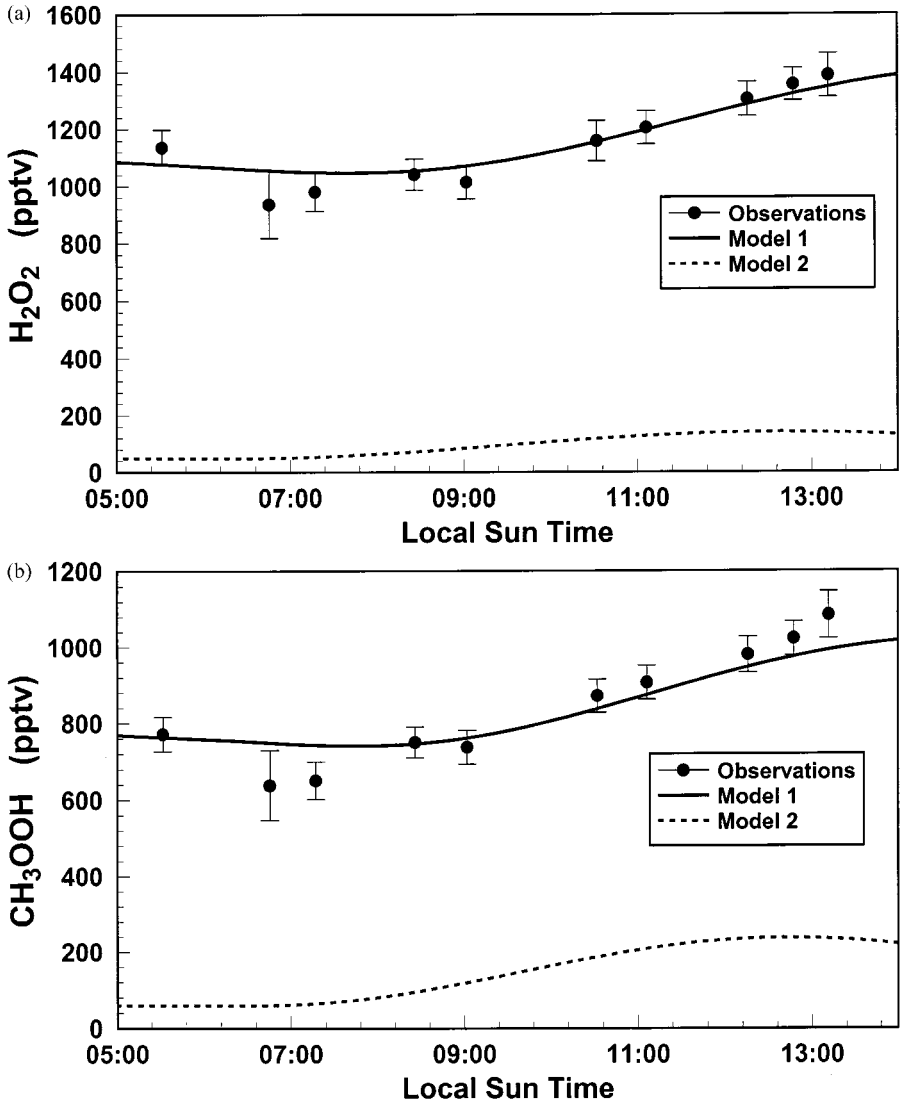


Figure 6. Comparison of model simulated and observed profiles for: (a) H_2O_2 (model 1: $k_{SL} = 9.8 \times 10^{-6}$ s^{-1} and model 2: $k_{SL} = 5.8 \times 10^{-4}$ s^{-1}) and (b) CH_3OOH (model 1: $k_{SL} = 1.1 \times 10^{-5}$ s^{-1} and model 2: $k_{SL} = 3.5 \times 10^{-4}$ s^{-1}). Symbols give the average and standard deviation of observations for each BL horizontal leg.

environment, the value of k_{SL} is limited to aerosol scavenging and rainout losses. Furthermore, due to the absence of rain during flight 7, the value of k_{SL} reduces to loss on sea-salt aerosols and cloud droplets. The results from our model simulations for the BuL produced first order loss rates of 1.8×10^{-6} sec^{-1} and $\leqslant 1.0 \times 10^{-7}$ sec^{-1} for H_2O_2 and CH_3OOH, respectively. These low values would thus seem to confirm the results given earlier that clearly indicate that aerosol scavenging of

peroxides is not predominantly controlled by the sticking coefficients $\alpha_{H_2O_2}$ and α_{CH_3OOH}. Instead, it appears to have a major dependence on the rate of aqueous phase chemistry. As further evidence of this fact, we have here estimated the uptake time of H_2O_2 to reach saturation in wet aerosols. If this time is very short, as suggested above, it would point toward aqueous phase chemistry as the controlling step rather than collisional loss based on sticking coefficients. In our test case we took the average liquid water content of seasalt particles to be 6×10^{-5} g/m^3 (e.g., Chameides and Stelson, 1992). When combined with the known solubility of H_2O_2 in H_2O and a value for $\alpha_{H_2O_2}$ of 0.07, uptake times of only 5 min were estimated. This means that unless a significant chemical loss of H_2O_2 occurs, hydrated particles rather quickly come into equilibrium with gas phase H_2O_2.

Assuming that the rate of aerosol scavenging is controlled by aqueous phase chemistry and considering the similarity in SO_2 levels and aerosol number/size distribution for both BL and BuL regions, we have here, as a first approximation, taken the BL aerosol scavenging rate to be similar to that estimated for the BuL. If true, this would suggest that aerosol scavenging defines only about 18% of the BL removal of H_2O_2. Given a BL height of 0.55 km and the previously cited first order BL loss rates for the peroxides, the estimated BL deposition velocities for H_2O_2 and CH_3OOH can be estimated to be 0.4 cm/sec for H_2O_2 and 0.6 cm/sec for CH_3OOH (e.g., within the uncertainties of our calculations the values are the same). Values within nearly a factor of 2 (i.e., 1.0 cm/sec for H_2O_2 and 0.6 cm/sec for CH_3OOH) were also arrived at using an independent approach described by Duce *et al.* (1991). These estimated total deposition velocities (representing the total rate of the physical removal) can be compared with those reported for H_2O_2 by Ayers *et al.* (1992, 1996), Thompson *et al.* (1993), and Heikes *et al.* (1986, 1996) which ranged from 0.5 to 1 cm/sec. Thus, the overlap with earlier work is seen as being reasonably good.

For our standard model, the lifetime of CH_3OOH was estimated to be $\sim$11 hours. Oxidation by OH was found to be the most important removal pathway, accounting for 50% of the total. Deposition to the ocean contributed another 40% and CH_3OOH photolysis defined the final 10%. Not surprisingly, the major source (i.e., 85%) was tied to the reaction of CH_3OO with HO_2 radicals, (R15), with transport of CH_3OOH from the BuL defining the remaining 15%. For H_2O_2 the lifetime was estimated to be nearly a factor of 1.5 longer than that for CH_3OOH, e.g., $\sim$17 hrs. Unlike CH_3OOH, about 63% of the BL H_2O_2 loss could be attributed to physical removal, with deposition to ocean defining the largest component. Oxidation by OH (R10), accounted for 21% and photolysis (R9), contributed the remaining 16%. The dominant source of H_2O_2 (i.e., 75%) was the HO_2 self reaction (R8), and transport from the BuL was found to make up the remaining 25%. Thus, the overall picture that emerges from this budget analysis is that CH_3OOH is largely controlled by photochemical processes; whereas, for H_2O_2 both photochemical and physical processes must be carefully considered in assessing the mixing ratio of this species in the tropical marine BL. In the specific case of CH_3OOH, the

good agreement between model simulations and the observations also suggests that important aspects of tropical marine BL CH_4 oxidation chemistry are reasonably well represented by current photochemical mechanisms.

Recall earlier in the text, model simulations were presented that explored the possible importance of HO_2 radical loss to the marine aerosol. The conclusion reached was that even for sticking coefficients as high as unity this loss pathway does not represent a significant HO_x sink. However, it was noted that this process could have a significant impact on HO_2 radical levels, and hence, via reaction (R8), on the mixing ratio of H_2O_2. Thus, in the absence of HO_2 measurements, experimental observations of H_2O_2 could serve as surrogate species for testing the extent to which HO_2 might be influenced by aerosol scavenging. With this goal in mind, several modeling runs were carried out using again a wide range of α_{HO_2} values, i.e., 0.0, 0.2, 0.4 and 1.0. Used in conjunction with the aerosol number/size distribution, these sticking coefficients resulted in HO_2 first order loss rates of 0.0, 1.3, 2.3, and 4.2×10^{-3} sec^{-1}, respectively. The corresponding diel average HO_2 levels were 1. 5, 1.3, 1.2, and 1.1×10^8 molec/cm^3. These HO_2 values represents a 0.0%, 10%, 16%, and 27% decrease in HO_2 relative to the standard model. In Figure 7 we have shown the impact from these HO_2 reductions as expressed in terms of projected levels of H_2O_2. For each case considered, the value of $k_{SL}(H_2O_2)$ was adjusted such that each simulated H_2O_2 profile reproduced the H_2O_2 values observed during the early morning hours. For comparison purposes, the 'standard model' H_2O_2 profile is also shown in Figure 7, i.e., $\alpha_{HO_2} = 0.0$. From these profiles it is quite apparent that for $\alpha_{HO_2} \geqslant 0.2$ the model generated H_2O_2 levels are considerably underestimated versus those observed. As discussed earlier, laboratory measurements of α_{HO_2} on aqueous aerosols have reported values as high as 0.2; but depending on aerosol composition, values of α_{HO_2} have also been found as low as 0.05. The results shown in Figure 7 represent the first effort to use field data to assess the value of α_{HO_2}. Our interpretation of these results is that for wet BL sea-salt particles α_{HO_2} values of $\leqslant 0.2$ are required to be consistent with the observational H_2O_2 data. If, however, the HO_2 scavenging process is assumed reversible, an upper limit for the net loss of this species by aerosol scavenging would be 1.3×10^3 sec^{-1}. This suggests that the maximum HO_x sink due to aerosol scavenging of HO_2 would be no larger than 10%.

4.4. O_3 ANALYSIS

The analysis of the flight 7 H_2O_2 and CH_3OOH data have shown that current model photochemical HO_x mechanisms, with simple parameterized transport, can reasonably well describe the diurnal variations of these two species. Here, the same type analyses is extended to the O_3 data. In this case the mass balance equation can be expressed as:

$$\frac{d[O_3]}{dt} = F(O_3) - D(O_3) - \frac{V_d}{h}[O_3] + \frac{M}{h}\left([O_3]_{BuL} - [O_3]\right). \tag{3}$$

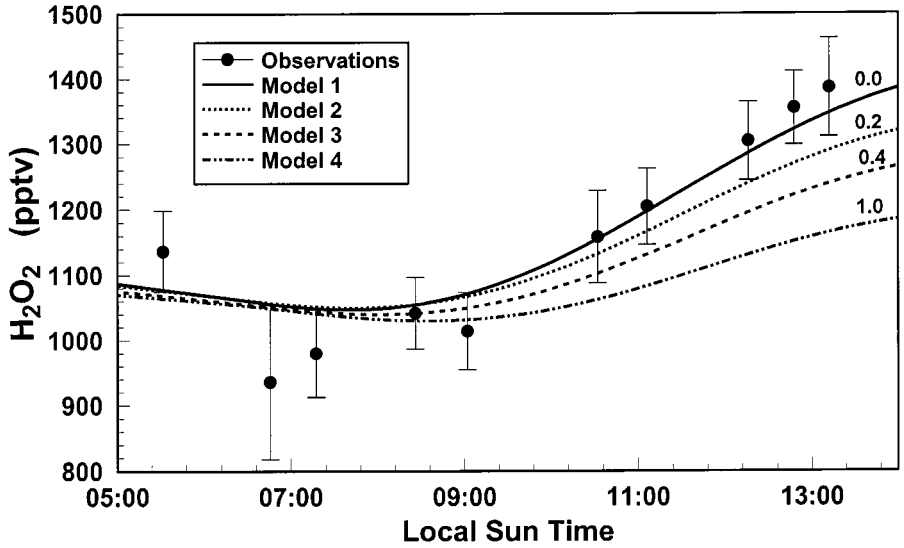


Figure 7. Sensitivity tests related to HO_2 heterogeneous loss on aerosol as reflected in levels of H_2O_2. Model 1: $\alpha(H_2O) = 0.0$, $k_{SL}(HO_2) = 0.0$; model 2: $\alpha(HO_2) = 0.2$, $k_{SL}(HO_2) = 1.3 \times 10^{-3}$ s^{-1}; model 3: $\alpha(HO_2) = 0.4$, $k_{SL}(HO_2) = 2.3 \times 10^{-3}$ s^{-1}; model 4: $\alpha(HO_2) = 1.0$, $k_{SL}(HO_2) = 4.2 \times 10^{-3}$ s^{-1}.

In Equation (3) $F(O_3)$ and $D(O_3)$ represent the BL rates of photochemical formation and destruction of O_3; 'V_d' is the dry deposition velocity; and 'h' denotes the height of the marine boundary layer. As before, 'M' is the mixing parameter used to account for the vertical mass exchange between the BL and BuL, and $[O_3]_{BuL}$ defines the buffer layer O_3 mixing ratio.

As in the peroxide simulations, all model runs designed to simulate diurnal profiles of O_3 were constrained by median values for all input parameters. As in the peroxide study, OH values were constrained to the flight 7 observations. The value of 'V_d' was set at 0.026 cm/sec as evaluated for marine conditions by Kawa and Pearson (1989). Reflecting the more limited sampling carried out in the BuL during flight 7, both the median value (i.e., 14 ppbv) from these observations as well as a range of test values for BuL O_3 were used in our O_3 simulations. As shown in Figure 8, the range of BuL O_3 values employed was 11 to 17 ppbv. From this figure, it can be seen that a key feature of the BL O_3 profile is its mid-morning maximum near 10:00 hrs. This maximum is consistent with the current thinking that tropical marine BL O_3 levels are controlled by a combination of downward transport serving as a source and photochemistry defining the major sink (e.g., Thompson *et al.*. 1993; Chen, 1995; Davis *et al.*, 1996; Jacob *et al.*, 1996; Crawford *et al.*, 1997a).

As revealed in Figure 8, our model simulations reproduce reasonably well the general features of the O_3 observational data. The level of agreement, however, is found to be quite dependent on the values assigned to the BuL O_3 mixing ratio.

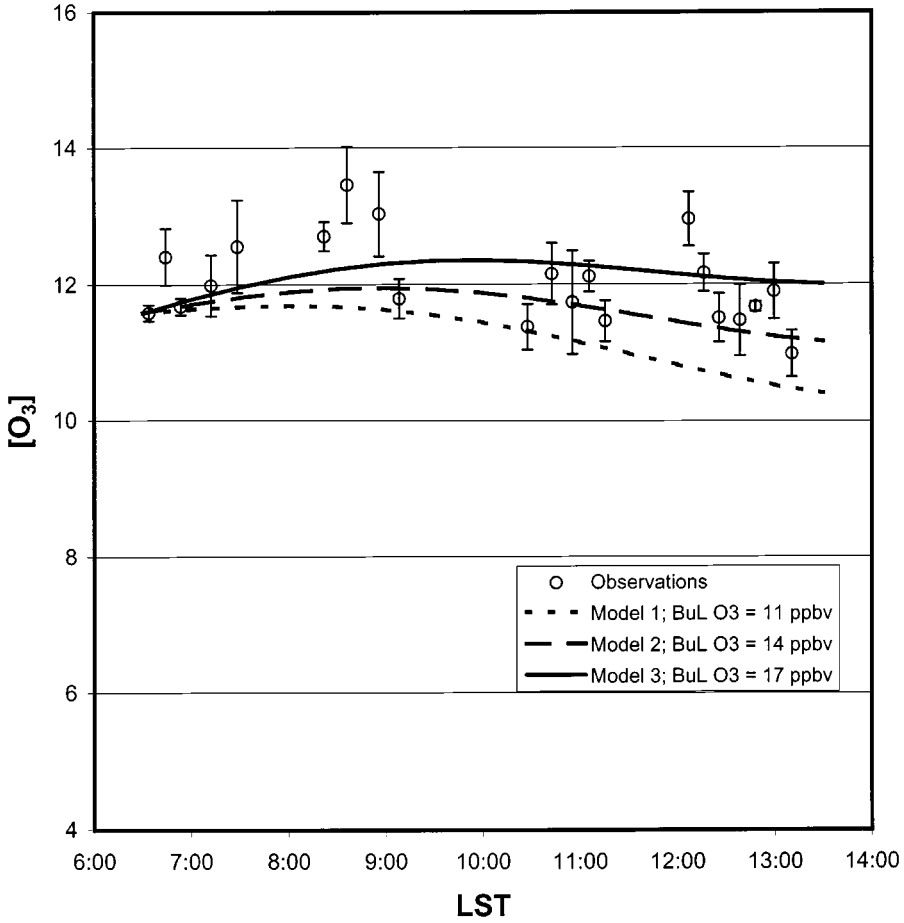


Figure 8. Comparison of model simulated and observed O_3 profiles. Symbols give the average and standard deviation of observations for each BL horizontal leg.

For a constant '*M*' value of 1.2 cm/sec, Figure 8 suggests that the best fit to the observations is achieved with a BuL O_3 value corresponding to the median value of 14 ppbv.

The estimated 24 hr average ozone formation and destruction rates for flight 7 were 0.8 and 2.7 ppbv/day, respectively. This means that the net effect of photochemistry (i.e., the O_3 tendency, $P(O_3)$) was –1.9 ppbv/day. This value is well within the range of BL values (i.e. –1 to –2 ppbv/day) reported by other investigators for MBL background tropical Pacific conditions (see e.g., Liu *et al.*, 1983; Davis *et al.*, 1996; Duderstadt *et al.*, 1998; Crawford *et al.*, 1999b; and references therein). Not surprisingly, the $O(^1D)$ plus H_2O reaction (R1), was found to be the dominant O_3 destruction process, contributing nearly 85% to the total. It was also determined that the photochemical O_3 destruction rate of 2.7 ppbv/day was approximately equal to the sum of the formation rates for the peroxides (i.e., H_2O_2

and CH_3OOH). This is consistent with the notion that OH free radicals formed via the $O(^1D)/H_2O$ reaction are quickly converted to HO_2 radicals by reaction (R3) and that these are subsequently lost in the self reaction (R8) as well as reaction with CH_3O_2 radicals. As previously observed by Ayers *et al.* (1992) and Penkett *et al.* (1997), a clear negative correlation can be seen between the levels of the peroxides and ozone. For the flight 7 data a regression analysis resulted in an R^2 value of $\sim$0.78.

5. Summary and Conclusion

This study has tested current mechanisms that are used to describe HO_x photochemistry by comparing model simulated profiles with observational data. The critical species involved in this comparison were OH, H_2O_2, CH_3OOH, and O_3. The database employed was that collected during NASA's PEM-Tropics A airborne field study. The major focus of this analysis was on those data recorded during P-3B flight 7 which mainly sampled from 50 to 300 km of Christmas Island in the central equatorial Pacific. An examination of the OH data recorded has shown that the difference between model simulations and the observations is within 15–20%, well below the possible range of systematic errors for both the observations (i.e., 20%) and model simulations (e.g., 25%). The observed diurnal profiles of H_2O_2 and CH_3OOH were also well reproduced in our simulations as reflected in minimum values in early morning hours and maximum values in mid afternoon. In addition, model profiles and observations of O_3 showed similar trends. In particular, the simulations reproduced the observed mid-morning peak in O_3. The results from these comparisons strongly suggests that current photochemical mechanisms do describe quite well many of the photochemical processes operating in a remote tropical marine BL setting.

A detailed analysis of HO_x sources and sinks was carried out using our standard model. The reaction of $O(^1D)$ with H_2O was shown to be the single most important HO_x source, e.g., 80% of the total. Transport of H_2O_2 and CH_3OOH from the BuL to the BL was also shown to play a significant role during flight 7, contributing $\sim$20% to the total. The two major losses of HO_x were shown to involve the species H_2O_2 and CH_3OOH, 39% and 53%, respectively. For H_2O_2, 75% of the loss was due to physical removal processes; whereas, for CH_3OOH only 43% was in this form.

The deposition velocities for H_2O_2 and CH_3OOH were estimated at 0.4 cm/sec for H_2O_2 and 0.6 cm/sec for CH_3OOH; however, within the model uncertainties for these simulations (i.e., factor of 1.5) the two values could be viewed as nearly identical. Our results indicate that CH_3OOH is largely controlled by photochemical processes, whereas H_2O_2 is controlled both by photochemistry and physical processes. Furthermore, our model simulations, constrained by *in situ* observations of peroxide made in both BL and BuL, also suggest that deposition to the ocean surface is most likely to be the dominant physical removal process of the peroxides

in the remote marine boundary layer. Aerosol scavenging may play only a minor role.

Concerning the heterogeneous loss HO_2 radicals our analysis would suggest an upper limit first order loss of no larger than 1.3×10^{-3} s^{-1}. This would represent at most a 10% additional sink for HO_x. In future studies a more refined analysis of the latter issue as well as several other aspects of HO_x chemistry would clearly benefit from having available not only observations of OH but also HO_2 and CH_2O.

References

Ayers, G. P., Penkett, S. A., Gillett, R. W., Bandy, B., Galbally, I. E., C. M. Meyer, Elsworth, M., Bentley, S. T., and Forgan, B. W., 1992: Photochemical production of hydrogen peroxides and destruction of ozone in marine air over the southern ocean, *Nature* **360**, 446–449.

Ayers, G. P., Penkett, S. A., Gillett, R. W., Bandy, B. J., Galbally, I. E., Meyer, C. P., Elsworth, M., Bentley, S. T., and Forgan, B. W., 1996: Annual cycle of peroxides and ozone in marine air at Cape Grim, Tasmania, *J. Atmos. Chem.* **23**, 221–252.

Bradshaw, J., Davis, D., Crawford, J., Chen, G., Shetter, R., Müller, M., Gregory, G. Sachse, G., Barrick, J., Blake, D., Heikes, B., Mastromarino, J., and Sandholm, S., 1999: Photofragmentation two-photon laser-induced fluorescence detection of NO_2 and NO: Comparison of measurements with model results based on airborne observations during PEM-Tropics A *Geophys. Res. Lett.* **26**, 471–474.

Brune, W. H., Faloona, I. C., Tan, D., Weinheimer, A. J., Campos, T., Ridley, B. A., Vay, S. A., Collins, J. E., Sachse, G. W., Jaeglé, L., and Jacob, D. J., 1998: Airborne in situ OH and HO_2 observations in the cloud-free troposphere and stratosphere during SUCCESS, *Geophys. Res. Lett.* **25**, 1701–1704.

Cantrell, C. A., Shetter, R. E., Gilpin, T. M., Calvert, J. G., Eisele, F. L., and Tanner, D. J., 1996: Peroxy radical concentrations measured and calculated from trace gas measurements in the Mauna Loa observatory photochemistry experiment 2, *J. Geophys. Res.* **101**, 14,653–14,664.

Chameides, W. L. and Davis, D. D., 1982: The free radical chemistry of cloud droplets and its impact upon the composition of rain, *J. Geophys. Res.* **87**, 4863–4877.

Chameides W. L., 1984: The photochemistry of a remote marine stratiform cloud, *J. Geophys. Res.*, **89**, 4739–4755.

Chameides W. L., Davis, D.D., Bradshaw, J.D., Sandholm, S., Rodgers, M. O., Baum, B., Ridley, R., G., Carroll, M. A., Gregory, G., Schiff, H., Hastie, D. B., Torres, A., and Condon, E., 1990: Observed and model-calculated NO_2/NO ratios in tropospheric air sampled during the NASA GTE/CITE 2 field study, *J. Geophys. Res.* **95**, 10,235–10,247.

Chameides, W. L. and Stelson, A. W., 1992: Aqueous-phase chemical processes in deliquescent sea-salt aerosols: A mechanism that couples the atmospheric cycles of S and sea salt, *J. Geophys. Res.* **97**, 20,565–20,580.

Chen, G., 1995: A study of tropospheric photochemistry in the subtropical/tropical North and South Atlantic, *Dissertation*, PhD Thesis, Georgia Inst. of Tech., Atlanta GA.

Clarke, A. D., Li, Z., and Litchy, M., 1996: Aerosol dynamics in the equatorial Pacific marine boundary layer: Microphysics, diurnal cycles, and entraiment, *Geophys. Res. Lett.* **23**, 733–736.

Clarke A. D., Eisele, F., Kapustin, V. N., Moore, K., Tanner, D., Mauldin, L., Litchy, M., Lienert, B., Carroll, M. A., and Albercook, G., 1999: Nucleation in the equatorial free troposphere: Favorable environments during PEM-Tropics, *J. Geophys. Res.* **104**, 5735–5744.

Crawford, J., Davis, D., Chen, G., Bradshaw, J., Sandholm, S., Gregory, G., Sachse, G., Anderson, B., Collins, J., Blake, D., Singh, H., Heikes, B., Talbot, R., and Rodriguez, J., 1996: Photostationary

state analysis of the NO_2-NO system based on airborne observations from the western and central North Pacific, *J. Geophys. Res.* **101**, 2053–2072.

Crawford, J., Davis, D. D., Chen, G., Bradshaw, J., Sandholm, S., Kondo, Y., Merrill, J., Liu, S., Browell, E., Gregory, G., Anderson, B., Sachse, G., Barrick, J., Blake, D., Talbot, R., and Pueschel, R., 1997a: Implications of large scale shifts in tropospheric NO, levels in the remote tropical Pacific, *J. Geophys. Res.* **102**, 28,447–28,468.

Crawford, J. H., Davis, D. D., Chen, G., Bradshaw, J., Sandholm, S., Kondo, Y., Liu, S., Browell, E., Gregory, G., Anderson, B., Sachse, G., Collins, J., Barrick, J., Blake, D., Talbot, R., and Singh, H., 1997b: An assessment of ozone photochemistry in the extratropical western north Pacific: Impact of continental outflow during the late winter/earlier spring, *J. Geophys. Res.* **102**, 28,469–28,487.

Crawford, J. D., Davis, Olson, J., Chen, G., Liu, S., Gregory, G., Barrick, J., Sachse, G., Sandholm, S., Heikes, B., Singh, H., and Blake, D., 1999a: Assessment of upper tropospheric HO_x sources over the tropical Pacific based on NASA GTE/PEM data: Net effect on HO_x and other photochemical parameters, *J. Geophys. Res.* **104**, 16,255–16,273.

Crawford, J., Davis, D., Chen, G., Shetter, R., Müller, M., Barrick, J., and Olson, J., 1999b: An assessment of cloud effects on photolysis rate coefficients: Comparison of experimental and theoretical values, *J. Geophys. Res.* **104**, 5725–5734.

Davis, D. D. *et al*., 1993: Photostationary state analysis of the NO_2-NO system based on airborne observations from the subtropical/tropical North and South Atlantic, *J. Geophys. Res.* **98**, 23,501–23,523.

Davis, D. D., Crawford, J., Chen, G., Chameides, W., Liu, S., Bradshaw, J., Sandholm, S., Sachse, G., Gregory, G., Anderson, B., Barrick, J., Bachmeier, A., Collins, J., Browell, E., Blake, D., Rowland, S., Kondo, Y., Singh, H., Talbot, R., Heikes, B., Merrill, J., Rodriguez, J., and Newell, R. E., 1996: Assessment of the ozone photochemistry tendency in the western North Pacific as inferred from PEM-West A observations during the fall of 1991, *J. Geophys. Res.* **101**, 2111–2134.

Davis, D., Chen, G., Bandy, A., Thornton, D., Eisele, F., Mauldin, L., Tanner, D., Lenschow, D., Fuelberg, H., Huebert, B., Heath, J., Clarke, A., and Blake, D.,: 1999: Dimethyl sulfide oxidation in the equatorial Pacific: Comparison of model simulations with field observations for DMS, SO_2, H_2SO_4(g), MSA(g), MS, and NSS, *J. Geophys. Res.* **104**, 5765–5784.

DeMore, W. B., Sander, S. P., Golden, D. M., Hampson, R. F., Kurylo, M. J., Howard, C. J., Ravishankara, A. R., Kolb, C. E., and Molina, M. J., 1997: Chemical kinetics and photochemical data for use in stratospheric modeling, *JPL Publ. 97-4*, Jet Propul. Lab., Pasadena, CA.

Duce, R. A. *et al*., 1991: The atmospheric input of trace species to the world ocean, *Global Biogeochemical Cycles* **5**, 193–260.

Duderstadt, K. A., Carroll, M. A., Sillman, S., Wang, T., Albercook, G. M., Feng, L., Parrish, D. D., Holloway, J. S., Felisenfeld, F. C., Blake, D. R., Blake, N. J., and Forbes, G., 1998: Photochemical production and loss rates of ozone at Sable Island, Nova Scotia during the North Atlantic Regional Experiment (NARE) 1993 Summer Intensive, *J. Geophys. Res.* **103**, 13,531–13,555.

Eisele, F. L. and Tanner, D. J., 1991: Ion assisted tropospheric OH measurement, *J. Geophys. Res*. **96**, 9295–9308.

Eisele, F. L. and Tanner, D. J., 1993: Measurement of the gas phase concentration of H_2SO_4 and methane sulfonic acid and estimates of H_2SO_4 production and loss in the atmosphere, *J. Geophys. Res*. **98**, 9001–9010.

Fan, S.-M., Jacob, D. J., Mauzerall, D. L., Bradshaw, J. D., Sandholm, S. T., Blake, D. R., Singh, H. B., Talbot, R. W., Gregory, G. L., and Sachse, G. W., 1994: Origin of tropospheric NO_x over subarctic eastern Canada in summer, *J. Geophys. Res*. **99**, 16,867–16,877.

Fuchs, N. A. and Sutugin, A. G., 1970: Highly Dispersed Aerosols, Ann Arbor Science Publishers, Ann Arbor, Michigan.

Hanson, D. R., Burkholder, J. B., Howard, C. J., and Ravishankara, A. R., 1992: Measurement of OH and HO_2 radical uptake coefficients on water and sulfuric acid surfaces, *J. Phys. Chem.* **96**, 4979–4985.

Harder, J. W., Jakoubek, R. 0., and Mount, G. H., 1997: Measuerment of tropospheric trace gases by long-path differential absorption spectroscopy during the 1993 OH photochemistry experiment, *J. Geophys. Res.* **102**, 6215–6226.

Heikes, B. G. and Thompson, A. M., 1983: Effects of heterogeneous processes on NO_3, HONO, and HNO_3, chemistry in the troposphere, *J. Geophys. Res.* **88**, 10,883–10,895.

Heikes, B. G., Delany, A. C., Lazarus, A. L., and Penkett, S. A., 1986: Measured surface flux of H_2O_2 to wheat, *Eos Trans. AGU* **67**, 885.

Heikes, B. G., 1992: Formaldehyde and hydroperoxides at Mauna-Loa observatory, *J. Geophys. Res.* **97**, 18,001–18,013.

Heikes, B. G., Lee, M., Bradshaw, J. D., Sandholm, S., Davis, S. D., Crawford, J. H., Jose Rodriguez, Liu, S., McKeen, S., Thornton, D., Bandy, A., Gregory, G., Talbot, R., and Blake, D., 1996a: Hydrogen peroxide and methylhydroperoxide distributions related to ozone and odd hydrogen over the North Pacific in the fall of 1991, *J. Geophys. Res.* **101**, 1891–1905.

Heikes, B. G., Lee, M., Jacob, D., Talbot, R., Bradshaw, J., Singh, H., Blake, D., Anderson, B., Fuelberg, H., and Thompson, A. M., 1996b: Ozone hydroperoxides oxides of nitrogen, and hydrocarbon budgets in the marine boundary layer over the South Atlantic, *J. Geophys. Res.*, **101**, 24,221–24,235.

Hoell, J. D., Davis, D. D., Jacob, D. J., Rodgers, M. O., Newell, R. E., Fuelberg, H. E., McNeal, R. J., Raper, J. L., and Bendura, R. J., 1999: Pacific exploratory mission in the tropics; September 1996, *J. Geophys. Res.* **104**, 5567–5583.

Jacob, D. J., 1986: Chemistry of OH in remote clouds and its role in the production of formic acid and peroxymonosulfate, *J. Geophys. Res.* **91**, 9807–9826.

Jacob, D. J., Heikes, B. G., Fan, S-M., Logan, J. A., Mauzerall, D. L., Bradshaw, J. D., Singh, H. B., Gregory, G. L., Talbot, R. W., Blake, D. R., and Sachse, G. W., 1996: The origin of ozone and NO, in the tropical troposphere: A photochemical analysis of aircraft observations over the south Atlantic basin, *J. Geophys. Res.* **101**, 24,235–24,250.

Kawa, S. R. and Pearson Jr., R., 1989: Ozone budgets from dynamics and chemistry of marine stratocumulus experiment, *J Geophys. Res.* **94**, 9809–9817.

Lee, M., Noone, B. C., O'Sullivan, D., and Heikes, B. G., 1995: Method for the collection and HPLC analysis of hydrogen peroxide and C_1 and C_2 hydroperoxides in the atmosphere, *J. Atmos. Ocean. Technol.* **12**, 1060–1070.

Levy, H., 1971: Normal atmosphere: Large radical and formaldehyde concentrations predicted, *Science* **173**, 141–143.

Levy, H., 1972: Photochemistry of the lower troposphere, *Planet. Space Sci.* **20**, 919–935.

Levy, H., 1974: Photochemistry of the troposphere, *Adv. Photo chem.* **9**, 369–524.

Liu, S. C., McFarland, M., Kley, D., Zafiriou, O., and Huebert, B., 1983: Tropospheric NO_x and O_3 budget in the equatorial Pacific, *J. Geophys. Res.* **88**, 1360–1368.

Liu, S. C. *et al.*, 1992: A study of the photochemistry and ozone budget during the Mauna Loa observatory photochemistry experiment, *J. Geophys. Res.* **97**, 10,463–10,471.

Magi, L., Schweitzer, F., Pallares, C., Cherif, S., Mirabel, P., and George, C., 1997: Investigation of the uptake rate of ozone and methyl hydroperoxide by water surfaces, *J. Phys. Chem.* **101**, 4943–4949.

Mauldin III, R. L., Frost, G. J., Chen, G., Tanner, D. J., Prevot, A. S. H., Davis, D. D., and Eisele, F. L., OH measurements during the first aerosol characterization experiment (ACE 1): Observations and model comparisons, *J. Geophys. Res.* **103**, 16,713–16,729.

Mauldin III, R. L., Tanner, D. J., and Eisele, F. L., 1999: Measurement of OH during during PEM tropics A, *J. Geophys. Res.* **104**, 5817–5827.

McPeters, R. D., Bhartia, P. K., Krueger, A. J., Herman, J. R., Wellemeyer, C. G., Seftor, C. J., Jaross, G., Torres, O., Moy, L., Labow, G., Byerly, W., Taylor, S. L., Swissler, T., and Cebula, R. P., 1998: Earth Probe total ozone mapping spectrometer (TOMS) data products user's guide, NASA/TP-1998-206895.

Mount, G. H., 1992: The measurement of tropospheric OH by long path absorption. 1. Instrumentation, *J. Geophys. Res.* **97**, 2427–2444.

Mozurkewich, M. and Calvert, J. G., 1998: Reaction probability of N_2O_5 on aqueous aerosols, *J. Geophys. Res.* **93**, 15,889–15,896.

Penkett, S. A., Monks, P. S., Carpenter, L. J., and Clemitshaw, K. C., Ayers, G. P., Gilett, R. W., Galbally, I. E., and Meyer, C. P., 1997: Relationships between ozone photolysis rates and peroxy radical concentrations in clean marine air over the Southern ocean, *J. Geophys. Res.* **102**, 12,805–12,817.

Penkett, S. A., Reeves, C. E., Bandy, B. J., Kent, J. M., and Richer, H. R., 1998: Comparison of calculated and measured peroxide data collected in marine air to investigate prominent features of the annual cycle of ozone in the troposphere, *J. Geophys. Res.* **103**, 13,377–13,388.

Ridley, B., Madronich, S., Chatfield, R., Walega, J., Shetter, R., Carroll, M., and Shetter, R., 1992: Measurements and model simulations of the photostationary state during the Mauna Loa observatory photochemistry experiment: Implications for radical concentrations and ozone production and loss rates, *J. Geophys. Res.* **97**, 10,375–10,388.

Russell, L. M., Lenschow, D. H., Laursen, K. K., Bates, T. S., Bandy, A. R., Thornton, D., 1998: Bidirectional mixing in a marine PBL overlain by a second turbulent layer, *J. Geophys. Res.* **103**, 16,411–16,432.

Schwartz, S. E. and Freiburg, J. E., 1981: Mass-transport limitation to the rate of reaction of gases in liquid droplets: Application to oxidation of SO_2 in aqueous solutions, *Atmos. Env.* **15**, 1129–1144.

Schwartz, S. E., 1984: Gas-aqueous reactions of sulfur and nitrogen oxides in liquid-water clouds, *SO_2, NO and NO_2 Oxidation Mechanisms: Atmospheric Considerations*, Butterworth, Boston, pp. 173–208.

Schwartz, S. E., 1986: Mass transport considerations pertinent to aqueous-phase reactions of gases in liquid water clouds, *Chemistry of Multiphase Atmospheric Systems*, Springer, Heidelburg, pp. 415–471.

Schwartz, S. E., 1988: Mass-transport limitation to the rate of in-cloud oxidation of SO_2: Reexamination in the light of new data, *Atmos. Env.* **22**, 2491–2499.

Talukdar, R. K., Longfellow, C. A., Gilles, M. K., and Ravishankara, A. R., 1998: Quantum yields of $O(^1D)$ in the photolysis of ozone between 289 and 329 nm as a function of temperature, *Geophys. Res. Lett* **25**, 143–146.

Tanner, D. J. and Eisele, F. L., 1995: Present OH measurement limits and associated uncertainties, *J. Geophys. Res.* **100**, 2883–2892.

Thompson, A. M. and Stewart, R. W., 1991: Effect of chemical kinetics uncertainties on calculated constituents in a tropospheric photochemical model, *J. Geophys. Res.* **96**, 13,089–13,108.

Thompson A. M., Johnson, J. E., Torres, A. L., Bates, T. S., Kelly, K. C., Atlas, E., Greenberg, J. P., Donahue, N. M., Yvon, S., Saltzman, E., Heikes, B. G., Mosher, B. W., Shashkov, A. A., and Yegorov, V. I., 1993: Ozone observations and a model of marine boundary layer photochemistry during SAGA 3, *J. Geophys. Res.* **98**, 16,955–16,968.

Torres, A. L. and Thompson, A. M., 1993: Nitric oxide in the equatorial Pacific boundary layer: SAGA 3 Measurements, *J. Geophys. Res.* **98**, 16,949–16,954.

Trainer, M. E., Hsie, Y., McKeen, S. A., Tallamraju, R., Parrish, D. D., Fehsenfeld, F. C., and Liu, S. C., 1987: Impact of natural hydrocarbons in hydroxyl and peroxy radicals at a remote site, *J. Geophys. Res.* **92**, 11,879–11,894.

Worsnop, D. R., Zahniser, M. S., Kolb, C. E., Gardner, J. A., Watson, L.R., Van Doren, J. M., Jayne, J. T., and Davidovits, P., 1989: Temperature dependance of mass accommodation of SO_2 and H_2O_2 on aqueous surfaces, *J. Phys. Chem.* **93**, 1159–1172.